Journal of the European Ceramic Society 39 (2019) 4011–4022

Contents lists available at ScienceDirect

Journal of the European Ceramic Society

journal homepage: www.elsevier.com/locate/jeurceramsoc

Original Article

Finite elements based approaches for the modelling of radial crack formation upon Vickers indentation in silicon nitride ceramics

Yuri Kadin[a,*], Mehdi Mazaheri[a], Vadim Zolotarevskiy[b], Charlotte Vieillard[a], Mark Hadfield[b]

[a] SKF Research & Technology Development, Nieuwegein, the Netherlands
[b] Department of Design and Engineering, Bournemouth University, Bournemouth, UK

ARTICLE INFO

Keywords:
Silicon nitride
Crack propagation
Drucker-Prager plasticity
Vickers indentation

ABSTRACT

By having superior properties silicon nitride ceramics can be considered as the state-of-the-art material in the bearing industry. Vickers indentation of this material is typically accompanied by formation of cracks visible on surface. Two Finite Elements models are developed in the current work: the first model is based on fracture mechanics and the second on cleavage stress criterion. Plastic behavior of silicon nitride is included in the modeling, and since little is known on the plasticity of this material, the Drucker-Prager model (used for non-metallic materials) along with the classical J_2-plasticity are explored. The results of the fracture mechanics based model correlate well with experimental results in terms of surface crack length. The numerical results in terms of the morphology of the indented zone (including cracks and plastic zone) are provided by the stress criterion based model, and these results correlate well too, with the experimental data.

1. Introduction

Hybrid bearings consist of steel rings and rolling elements made of ceramics such as silicon nitride (Si_3N_4). The latter makes them beneficial over full steel bearings in multiple aspects, which is mainly due to superior mechanical properties of Si_3N_4 [1]. Compared to the traditional bearing material – steel, Si_3N_4 is lighter (which is important in aerospace applications), has higher hardness (providing high wear resistance) and higher stiffness (beneficial in high precision bearings). Other properties of Si_3N_4 [1], like good resistance to corrosion, low thermal expansion and high electrical insulation make hybrid bearings attractive for many of demanding applications. Ceramic components are not exposed to hydrogen embrittlement, while in steel components of bearings (see e.g [2,3]) it can be a case. Thanks to all these interesting properties it was shown that hybrid bearings have better performance in poor lubrication and contaminated conditions [4]. However compared to bearing steels, Si_3N_4 is still less resistant to fracture and fatigue crack propagation. Therefore, the investigation of nature of fracture in Si_3N_4 in attempt to improve its resistance to cracking, has potential interest in bearing industry.

Indentation testing is common for examining mechanical properties of ceramics, and it is typically performed by diamond sharp indenters, like Vickers, Knoop, etc. During indentation of ceramic materials, localized fracture can occur, which in some cases is manifested by cracks with well-defined geometry. In such cases, the indentation test can be used for the identification of toughness (see e.g. [5]), which is estimated as the function of hardness, elastic modulus and the surface size of cracks, which emanate from indent and can be easily visualized and measured. Indentation of Si_3N_4 can be also used for the creation of artificial defects mimicking surface flaws in ceramic rolling elements [6–8] under rolling contact.

In literature, different theoretical approaches can be found for modelling of crack formation under indentation contact. Typically it is done by the Finite Elements (FE) method incorporating fracture mechanics into model [9–11], or by using advanced computational methods like X-FEM by which crack propagation can be simulated based on the cohesive behavior of material [12–15]. Since the indentation process is inevitably accompanied by irreversible deformation (resulting in residual indent), plasticity should be included into the modelling. However in the case of Si_3N_4, which, in general, is considered as non-ductile material and which can experience only localized plasticity, modelling of plastic behavior is supposed to be rather complex and ambiguous. The classical J_2-plasticity, which excludes the hydrostatic stress effect on plastic deformation and is used for metals, can be inadequate for non-metallic materials which plastic behavior is dependent on the hydrostatic stress as result of their microstructure. More general model, termed as the Drucker-Prager (DP) plasticity, accounting for the hydrostatic stress and volumetric change in a plastic

* Corresponding author.
E-mail address: yuri.kadin@skf.com (Y. Kadin).

https://doi.org/10.1016/j.jeurceramsoc.2019.05.058
Received 16 November 2018; Received in revised form 10 May 2019; Accepted 28 May 2019
Available online 29 May 2019

range, is used for such materials as clayey soil [16], concrete [17], rock [18], etc. Regarding silicon nitride, it was reported in [19] that the DP plasticity in ductile regime is inherent for this material, and the DP model was used for the FE simulations of machining process, in which Si_3N_4 undergoes localized plasticity under cutting. Thus, it can be reasonably assumed that similar plastic behavior can be experienced by Si_3N_4 under sharp Vickers indentation.

The two FE based models are developed in the current work to simulate the Vickers crack formation: the fracture mechanics based model and the stress criterion based model. The first approach is based on the assumption that a Vickers crack appears at the completion of the unloading stage, meaning that its formation is entirely driven by tensile residual stress, which remain locked in the elastic-plastic body after the load is removed. Indeed, at this instance tensile stress gets its maximum, because prior to the full unloading tensile residual stress is partially neutralized by compressive stress induced by contact pressure. Since cracking in ceramic materials is predominantly driven by tension, such assumption can be accepted (see e.g. [20]), even though the process of crack formation prior to the unloading completion is totally overlooked. The crack analysis in this model is based on fracture mechanics, for which a radial crack of semi-elliptical shape was assumed [15]. This assumption is justified by our experimental observations and the examination of crack shape in [21] and [22]. The DP plasticity model is explored in this approach with respect to the FE simulation of Vickers indentation resulting in the formation of radial cracks in Si_3N_4.

In addition to the fracture mechanics based model, the formation of radial cracks is simulated here by the FE model incorporating the tensile stress failure criterion, for predicting the cleavage of Si_3N_4 (in literature it is known as the Rankine criterion). This approach can be seen as the simplification of the cohesive zone method which is frequently implemented in FE for the modelling of crack propagation. The stress criterion based model, relaxes the main assumption of the previous model by considering that the crack formation can occurs during the entire loading-unloading process.

Finally, the numerical results of both models are compared with the Vickers indentation experiment for the verification of the FE modelling and for the selection of proper plasticity model. The comparison is done in terms of the morphology of the indented zone, including the geometry of the crack, residual Vickers indent and plastic zone.

2. Vickers indentation and cracking

The schematic of the Vickers indentation problem is given in Fig. 1a. The vertical load, P, is applied on the indenter of pyramid shape, which hardness significantly exceeds the hardness of a Si_3N_4 substrate. Under the contact with sharp indenter localized plastic flow in Si_3N_4 takes a place which leads to the formation of a plastic zone, enveloping the indent, as is schematically shown in Fig. 1b. This plastic zone is surrounded by tensile stresses, which develop due to incompressibility of plastically deformed material (see Fig. 1b). At this regime, the material deformed by compressive stress, behaves as a pressurized liquid inside a vessel, which causes tension in the vessel's shell. Such analogy was proposed by others (see e.g. [23,24]) in order to explain the phenomenon of crack formation under indentation contact (see Fig. 1c). Note, that the highest level of tensile stress is developed at the completion of the unloading stage (residual stress), because during the loading stage, when the substrate is in a contact with the indenter, the tensile stress surrounding the plastic zone is partially neutralized by compressive stress.

The geometry of radial cracks formed in the Vickers indentation is presented in Fig. 1c. The surface length of the radial crack is denoted by C_R and its depth by d_R. These cracks emanate from the sharp corners of the Vickers indent, which size is denoted by d. It should be noted that indentation can lead to formation of other types of cracks in brittle materials, like for example, C-cracks [25], subsurface lateral cracks [26], and the so-called Palmqvist cracks [21] which have half-penny shape and which appearance frequently precedes the radial cracks formation. In the current study, experimental exploration of the Vickers cracks morphology in Si_3N_4, revealed only presence of radial cracks, regardless the magnitude of indentation load.

It is not new to model plastic indentation by FE, however in the current case such analysis faces some difficulties, because little is known on the plasticity of Si_3N_4. Although Si_3N_4 is not a ductile material, certain plastic behavior is inherent to this material, too. Generally speaking, all materials, even very brittle, experience some limited plasticity, however, behavior of these materials in the plastic range can be rather different from the plastic behavior of metals, typically obeying the classical J_2-plasticity. It is acceptable to simulate plasticity of non-metallic materials by the Drucker-Prager (DP) model, which differs from the J_2-plasticity in the sense that it accounts for the hydrostatic stress effect. The difference between the two models is demonstrated in Fig. 2. The yield criterion is defined in terms of the equivalent von Mises stress, t, and the hydrostatic stress, p. While in the case of J_2-plasticity, p has no effect on yielding (see Fig. 2b), the DP model postulates that the hydrostatic stress strengthens material in compression and weakens it in tension (see Fig. 2a). The angle β, termed as the friction angle, determines how strong the hydrostatic stress influences (linearly) the yield limit. Obviously, in the case of J_2-plasticity the friction angle equals to 0. The fact that the material yield strength is dependent on p, means that the material volume increases during plastic deformation. This phenomenon is known as "dilation", and it corresponds to the expansion (or loosening) of material due to shear stress, which is indeed observed in some heterogeneous materials [16]. The volume dilation is defined by the angle, Ψ, (see Fig. 2a) and if this angle is different from the friction angle, β, it will lead to non-associated plasticity, which is out of the current study scope. Here, the simple DP model (β = Ψ), utilizing associated plasticity is used. The yield function, F_y, in this case is defined by the two material parameters, β and σ_y (yield limit in the absence of hydrostatic stress), as:

$$F_y = t - p\tan\beta - \sigma_y \tag{1}$$

The transition from the elastic to the plastic regime (yielding) occurs at the instance of $F_y = 0$. Note, that in the case of J_2-plasticty, the yield function is defined by a single material parameter, σ_y, and Eq. (1) simplifies to $F_y = t\text{-}\sigma_y$.

The peculiarity of the sharp indentation and its apparent difference from the spherical elastic-plastic contact [27] is due to the self-similarity of the problem with respect to the indentation load. It can be confirmed based on the well-known π-theorem (see e.g. [28]), stating that the number of dimensionless parameters governing any physical model, equals to the number of dimensional parameters minus the number of physical dimensions defining the model. In the current problem this theorem can be utilized with respect to the evaluation of the average contact pressure, p_{avg}, defined as P/A, (A is the contact area). Note, that at the first approximation it can be assumed that p_{avg} equals to hardness (for the proper hardness estimation the contact area, A, is measured after the load is removed). In the dimensional form the following equation can be formulated:

$$f(p_{avg},\ \sigma_y,\ \beta,\ E,\ \nu,\ P,\ \varphi) = 0 \tag{2}$$

In Eq. (2), E is the Young's modulus and ν is the Poisson's ratio of the indented material (the plastic properties of the material are defined by σ_y and β). The geometry of the sharp indenter (assumed in the current work as rigid) is defined by the angle, φ, which being prescribed by the Vickers test standard, is fixed in the current study. It is stated by Eq. (2), that the model is governed by the 7 parameters which are characterized by the 2 physical dimensions: for example, by the units of force, [N], (indentation load, P) and the units of stress [Pa] (the parameters p_{avg}, E and σ_y); the rest of the parameters in Eq. (2) (β, ν and φ) are dimensionless. According to the π-theorem it means that the current problem in the dimensionless form is governed by 5 dimensionless

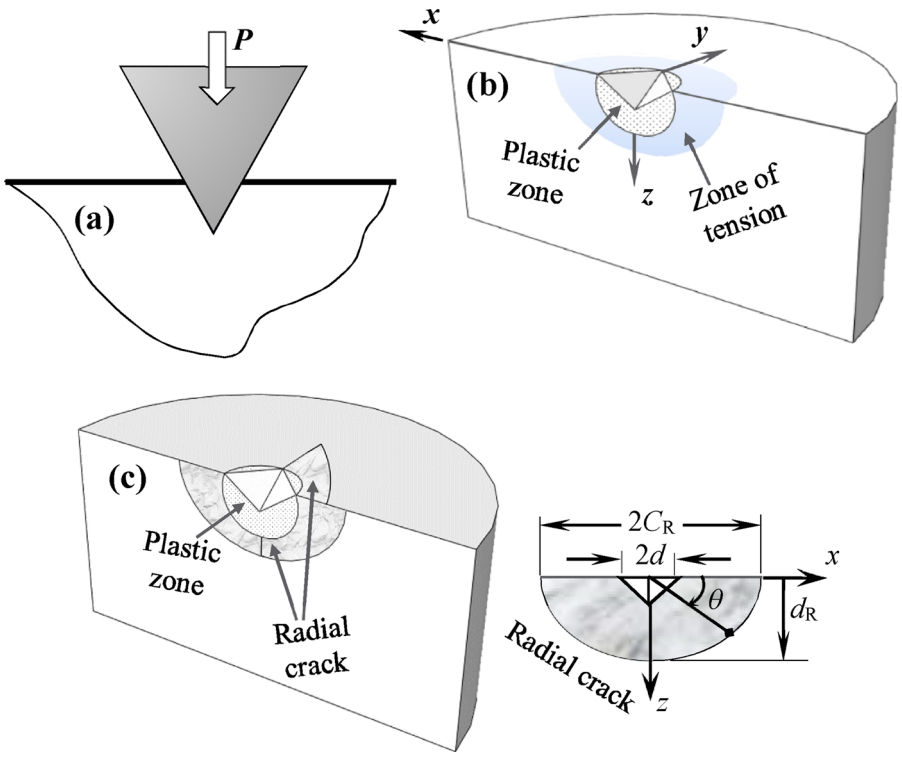

Fig. 1. Schematic of Vickers indentation and radial crack formation problem.

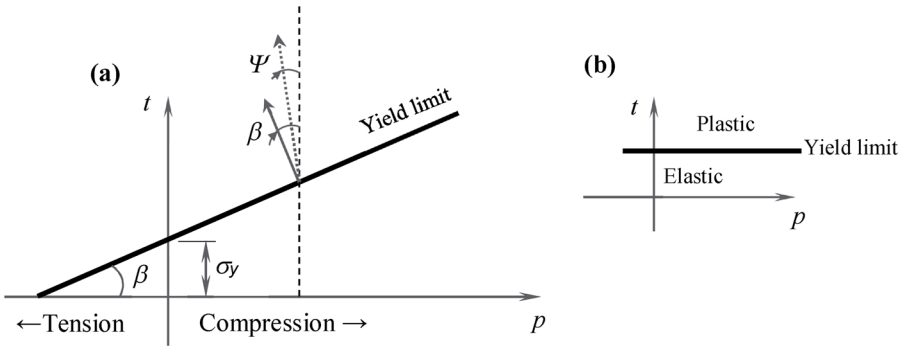

Fig. 2. Schematic of the DP plasticity model (a) and its comparison to the J_2-plasticty (b).

parameters. Hence, without loss of generality, Eq. (2) can be reformulated in the dimensionless form:

$$F\left(\frac{p_{avg}}{\sigma_y},\ \frac{\sigma_y}{E},\ \beta,\ \nu,\ \varphi\right) = 0 \tag{3}$$

It is important to note, that Eq. (3) does not include the indentation load, P, because no any dimensionless parameter can be created from this term. The indentation load is the single parameter in the model having the units of force, and since the model has no parameter of units of length, the dimensionless load cannot be created. This means that the average contact pressure, p_{avg}, and the subsurface stresses (which are supposed to be proportional to p_{avg}) are independent on the indentation load. On the other hand, the spherical contact problem is not self-similar with respect to the contact load [27], which is due to the presence of a geometrical parameter – radius of sphere – having the units of length. The geometry of a sharp indenter, however, is defined by the angle, φ – the dimensionless parameter.

Furthermore, the coordinate vector, $\mathbf{X}=[x, y, z]$, which is used to define the stress field, can be normalized by the indent size, d, in order to develop universal (independent on load) solution for the stress field, $\boldsymbol{\sigma}(\mathbf{X}/d)$, in the indented substrate. According to Eq. (3) the average contact pressure is proportional to σ_y and can be defined in the following form:

$$\sigma_{avg} = \sigma_y F_1\left(\frac{\sigma_y}{E},\ \beta,\ \nu,\ \varphi\right) \tag{4}$$

The solution for the stress field, can be defined as:

$$\boldsymbol{\sigma} = \sigma_y F_2\left(\frac{\mathbf{X}}{d},\ \frac{\sigma_y}{E},\ \beta,\ \nu,\ \varphi\right) \tag{5}$$

Recall, that p_{avg} is roughly equal to hardness, so according to the classical Tabor approach [29], F_1, is supposed to be close to 3. However using the FE analysis the dimensionless functions F_1 and F_2, in Eqs. (4) and (5) can be accurately computed. The indent size, d, can be calculated from a simple mechanical equilibrium, as:

$$d = \sqrt{\frac{P}{2p_{avg}}} = \sqrt{\frac{P}{2\xi H}} \tag{6}$$

The coefficient ξ in Eq. (6) defines the ratio between the actual material hardness and p_{avg}. These two parameters are not exactly equal to each other, because the indent size in a hardness test is measured after unloading.

The distribution of K_I along the front of a radial crack is calculated by the integration of the stress (perpendicular to the crack faces) over the crack domain. Manipulating with Eq. (5), it can be shown that, the K_I distribution along the crack front can be defined in the following form [10]:

$$K_I = \sigma_y \sqrt{C_R}\, F_3\left(\frac{\sigma_y}{E},\ \beta,\ \nu,\ \varphi,\ \frac{C_R}{d},\ \frac{d_R}{d},\ \theta\right) \tag{7}$$

In Eq. (7), the angle θ defines the coordinate along the crack front (see Fig. 1c). Since the current model aims to predict the surface crack length, C_R, (which can be easily measured in experiment), it is assumed here that the d_R/C_R ratio can be fixed. Moreover, it is obvious that d_R/C_R (the dimensionless crack depth) mainly affects K_I at the crack bottom ($\theta = 90^\circ$), however has negligible effect on K_I at the surface ($\theta = 0^\circ$), which is needed in the current analysis for the prediction of the surface length of the crack (see Fig. 1c).

3. Modelling techniques

3.1. Fracture mechanics based model

The DP plasticity is utilised in the current model for the simulation of indentation, which is not a new topic but has been already explored in some previous studies. In [30], the process of spherical indentation was modelled by FE in order to identify the material parameters associated with the DP model in highly porous inorganic solids (e.g. gypsum) by using the instrumented micro-indentation and the solution of inverse problem. Similar analysis was presented in [31] for the sharp nanoindentation and in [32] for spherical indentation of amorphous materials.

In the current work the Vickers indentation is parametrically studied by FE for different combinations of the DP model (β and σ_y). From this study, the average contact pressure, p_{avg}, as the function of β and σ_y is numerically evaluated. Further, such combinations of β and σ_y are selected for which the resultant p_{avg} value is close to the actual material hardness, H. Further, the crack formation problem is solved only for these combinations, and it is done by numerical computation of K_I. For this, the residual stresses, developed in the indented body after the completion of the unloading stage (computed by the elastic-plastic model), are mapped to the new model (elastic) containing a radial crack. In the latter model, the new equilibrium stress state is computed by FE for the problem with the new boundary conditions, resulted by the presence of the radial crack. The K_I evaluation is done by the crack opening displacement method (see e.g. [33]), for which the displacement field computed by the elastic FE model is used. Since K_I is evaluated on a free surface ($\theta = 0^\circ$, see again Fig. 1), the plane-stress conditions are utilised in the crack opening displacement method. Eventually, K_I as the function of the crack length, C_R, is evaluated.

The crack size prediction by the construction of the K_I vs. C_R curve is presented in Fig. 3. Recall, that K_I in the current analysis is evaluated at the crack tip located on the surface, and the K_I value at this tip is denoted here as K_I^0. The plastic zone, which geometry is computed in the indentation phase, is created in the elastic FE model along with the radial crack. While the geometry of the plastic zone and the crack depth, d_R, are fixed, the surface crack length, C_R, in the FE model changes from its smallest size, C_R^1, to the largest one, C_R^n, as is presented in Fig. 3a. The surface length of the radial crack is predicted by comparing the function $K_I^0 = f(C_R)$ to K_{IC}, as is schematically presented in Fig. 3b. The condition $K_I^0 = K_{IC}$ defines the crack arrest, or in the other words, the maximum crack size, C_R^*, to which it can propagate in the material having the toughness equal to K_{IC}. Strictly speaking, K_{IC} value is not constant but is dependent on the crack size, due to the so-called "short crack effect". However this effect is essential only for short cracks, which size is considerably lower than the critical size of the crack, C_0, which can be defined, as [34]:

$$C_0 = \frac{1}{\pi}\left(\frac{K_{IC}}{1.12\sigma_f}\right)^2 \tag{8}$$

where σ_f is the fracture strength of material at the micro-volume scale. For the typical properties of Si_3N_4, like K_{IC} is in a range of 5.5 to 6.5 [MPa·m$^{1/2}$] (see [35] and [36]) and σ_f in the range of 1200 to 1500 [MPa] (see [37] and [38]), C_0 according to Eq. (8) is in the range of 3.5 to 7.5 [μm], which is much smaller than the crack size observed in the Vickers indentation (few tens of microns). Hence, the short crack effect is excluded from the current analysis.

The modelling is done here by the commercial FE software ABAQUS, which is powerful and robust tool for simulation of plasticity, contact, etc. The FE models for the implementation of the current modelling technique are presented in Fig. 4. The elastic-plastic model for the simulation of the Vickers indentation is presented in Fig. 4a. The elastic-plastic substrate is discretised by the mesh of non-uniform density: at the contact zone, where the indentation and the plastic flow occur it has higher density than out of this zone. In total, the substrate is meshed by around 34,000 linear elements, which was found to be sufficient by performing the stress analysis with the varying mesh density. Since the diamond indenter is much harder than the Si_3N_4 substrate it is assumed that the indenter in the current FE model is absolutely rigid. The following elastic properties of Si_3N_4 are used here: E = 305 [GPa] and ν = 0.27 [38]. Since little is known on the Si_3N_4 plasticity, it assumed that it obeys the simple bilinear model and that the hardening is negligibly low: 0.2% of E, which is close to the so-called perfect plasticity. The plastic properties of the indented material (β and σ_y) are not fixed but vary for the parametric study. Due to the symmetry of the Vickers indentation problem, only one quarter of the substrate and the indenter are modelled. The symmetry boundary conditions are applied to the nodes located on the symmetry planes XZ and YZ (see Fig. 4a).

The FE model presented in Fig. 4b is used for the evaluation of K_I. This model is elastic (again, E = 305 [GPa] and ν = 0.27) and

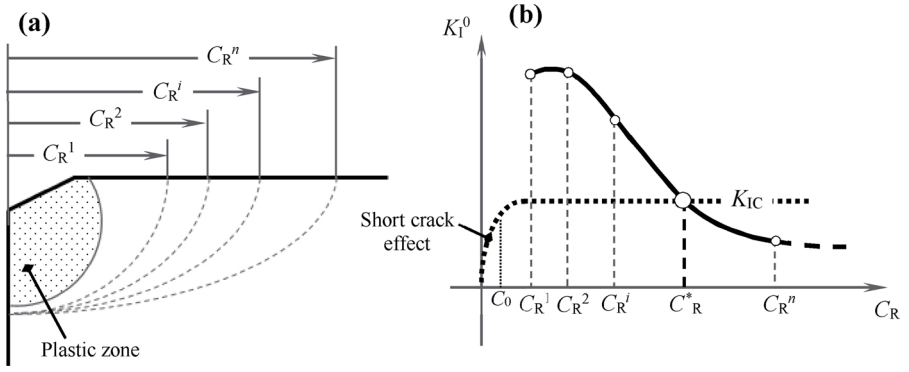

Fig. 3. Schematic of a radial crack modelling by FE (a) and the prediction of the crack size (b).

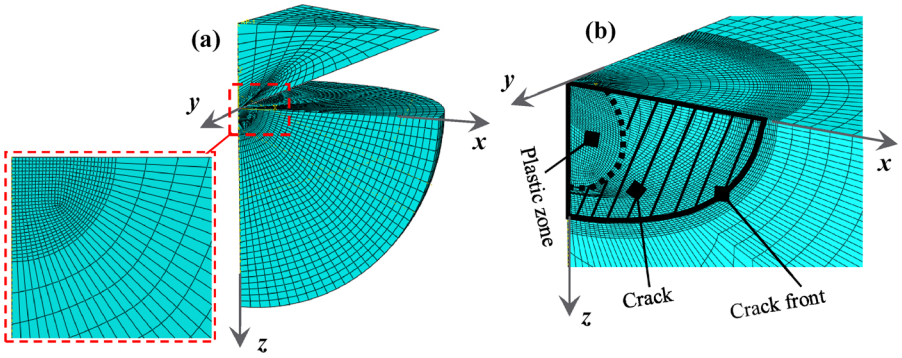

Fig. 4. FE models for treating the crack formation problem by fracture mechanics. The elastic-plastic model for the simulation of Vickers indentation (a) and the elastic model for the radial crack (hatched region) analysis (b).

differently from the previous model which is created once, the elastic model has to be updated with respect to the varying surface length of the crack (which is shown by the hatched area in Fig. 4b). The mesh configuration is updated too, in order to provide high mesh density along the crack front. The crack definition in the current model is based on the symmetry considerations: the nodes belonging to the crack (hatched zone in Fig. 4b) are free of the symmetry boundary conditions. Therefore, these nodes are free to move perpendicularly to the symmetry plane which mimics the opening of the radial crack under residual tensile stress. The stress field is mapped from the elastic-plastic (without crack) to the elastic (with crack) model by the standard ABAQUS function *Map solution.

Finally note, that the current methodology (fracture mechanics based approach) assumes, that the radial crack formation in the Vickers indentation is entirely driven by residual stresses. However, the crack initiation and its propagation prior to the unloading completion is overlooked by the current modelling approach. The alternative modelling approach, presented in the next sub-chapter, simulates the crack propagation during the entire loading-unloading cycle.

3.2. Stress criterion based model

Tensile stress criterion, known as the Rankine failure criterion, is used here to predict the formation of radial crack in Si_3N_4 under the Vickers indentation The Rankine criterion is used for brittle materials, and according to this criterion, cleavage occurs when the tensile stress, σ_t, exceeds the tensile fracture strength of material: $\sigma_t > \sigma_f$.

The algorithm of the current modelling approach is schematically presented in Fig. 5. This approach is based on the symmetry boundary consideration for which again, only one quarter of the substrate and the indenter are considered (see Fig. 6). By releasing the symmetry boundary conditions (the displacement U_x and the displacement U_y are equal to zero on the plane *YZ* and the plane *XZ,* respectively), the crack propagation is modelled (see Fig. 6). The symmetry boundary conditions are removed gradually, as the indentation load increases during the loading or decreases during the unloading stage. The load incrementally changes by small steps, and after each increment the tensile stress at each node on the symmetry planes is identified. If the tensile stress at a certain node exceeds the fracture strength, σ_t, the symmetry boundary conditions are removed from this node, meaning that material at this point is cracked. The solution is restarted for the next step with the new boundary conditions, corresponding to the model with a larger crack (propagated in the previous step). The restart is implemented by the standard options of the ABAQUS solver (function *Restart). The FE mesh used in the current approach (see Fig. 6) is identical to the mesh of the elastic-plastic FE model used in the fracture mechanics based approach.

The two rigid blocks are added to the model, as is shown in Fig. 6, and these blocks are in the frictionless contact with the symmetry planes of the indented substrate. These blocks aim to prevent non-physical crack behavior by blocking the motion of the nodes in the negative *x* (on the symmetry plane *YZ*) and *y* (on the symmetry plane *XZ*) directions (see Fig. 6). By this, the penetration of crack faces into each other (which is obviously not realistic) is prevented.

The fracture strength, σ_f, of Si_3N_4, needed for the current modelling approach, is estimated here from the cohesive zone model, which can be evaluated from the R-curve of material (see [35] and [37]). The cohesive zone model relates separation to traction, as is shown in Fig. 7, and according to [35] the Si_3N ceramics with toughness similar to the current one ($\approx$5.5 [MPa·m$^{1/2}$]) has the traction value at the peak around 1.25 [GPa] [37]. This maximum stress value is considered in the current work as the fracture strength, σ_f (see Fig. 7). In [36] and [37] using the cyclic loading experiment under the maximum load which is slightly below the critical one (causing instantaneous fracture), it was found that for $\sigma_f = 1.25$ [GPa], the length of the cohesive strip is around 7 [μm]. And this length is comparable to the distance of crack extension per cycle [36]. It is also important to note, that according to the formalism of the FE method the stress values are computed at the integration points. To convert them to the values at the nodes (as is required in the current approach) the averaging technique is used here being implemented by the ABAQUS programming environment. Due to such numerical implementation the current stress criterion can be seen as a non-local criterion predicting fracture due to the stress averaged over certain size [34]. For $K_{IC} = 5.5$ [MPa·m$^{1/2}$] and $\sigma_f = 1.25$ [GPa] the critical distance, C_0, according to Eq. (8) is around 5 [μm]. The element size in the fine mesh zone (see Fig. 6) is around 6.5 [μm] which is comparable to the critical distance and the cohesive strip length (around 7 [μm]). This means that the current FE model is reasonable not only from the numerical (sufficient accuracy) but also from the material (tensile stresses causing fracture are averaged over the size appropriate for the current material) point of view (Fig. 8).

Finally note, that the current modelling approach can be seen as a simplification of the modelling by cohesive elements for which a traction-separation law of material is used (see again Fig. 7). As result of this simplification, the current modelling technique, being based on the stress criterion, neglects the traction-separation behavior of material at the crack tip. This simplification is beneficial because it prevents any convergence problems associated with snap-back instability, inherent to cohesive behavior [39]. The poor convergence, caused by this instability, is typically improved by adding artificial viscosity, or by using dynamic implicit or explicit solver, which obviously costs computational time.

4. Experiment

A bearing grade silicon nitride materials have been used (Class I Si_3N_4, ISO 26602). The Vickers indentation tests were carried out on the carefully polished surfaces of silicon nitride materials for rolling

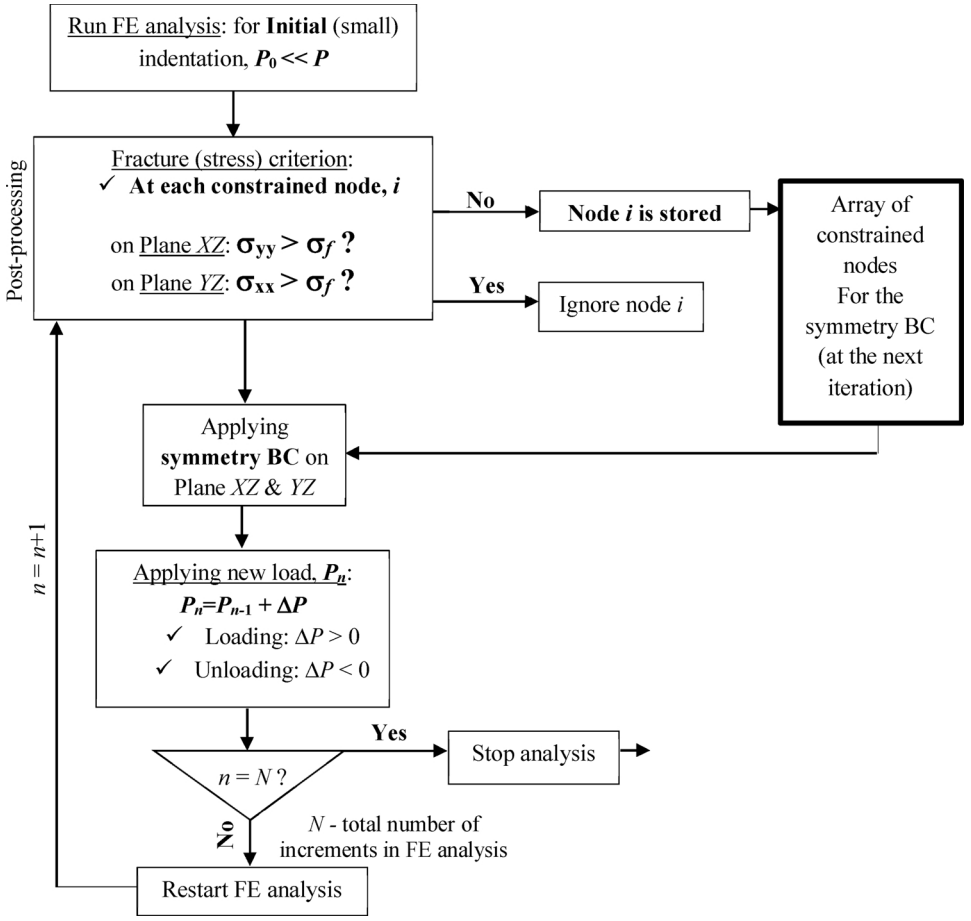

Fig. 5. Solution algorithm for the modelling of Vickers crack formation based on the tensile stress (Rankine) criterion.

elements. The ball bearings were cut, and polished using 15, 9, 3 μm diamond paste. The indentations were carried out using Zwick 3212 hardness measurement equipment. Wide range of indentation loads (10, 5, 3 and 1 kg) has been applied on the polished surfaces. Different parameters related to the radial cracks, C_R and d_R, (see Fig. 1) were measured using progressive polishing of the indent. The radial cracks are usually very closed in the surfaces, therefore the actual length of the cracks can be underestimated using classical bright field microscopy. To avoid this, UV fluorescent dye penetrant inspection method has been used. The penetrant is applied on the test sample, and the cracks can be

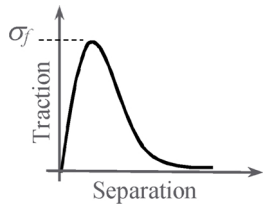

Fig. 7. Schematic of a traction-separation curve defining the fracture behavior of material according to the cohesive zone model.

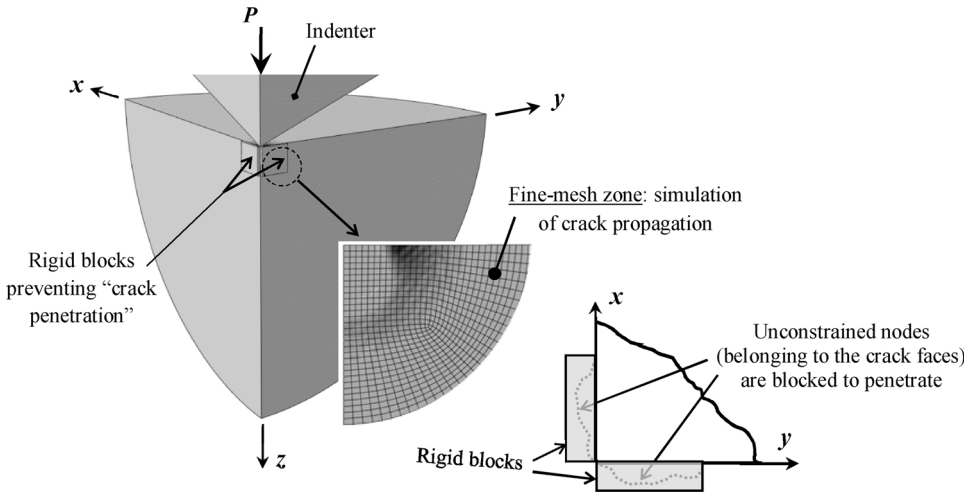

Fig. 6. FE model for the simulation of Vickers crack formation based on the tensile stress (Rankine) criterion.

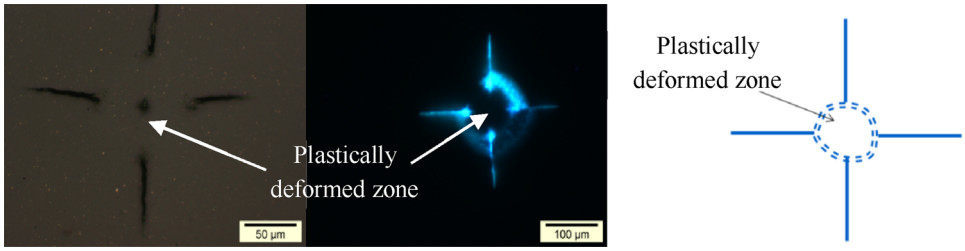

Fig. 8. Plastic zone identification.

observed using an optical microscopy equipped with a UV-lamp.

Hardness measurements were carried out using the indentation method. The tests were carried out with a diamond Vickers indenter under 10 [kgf] load with a dwell of 20 [sec] on carefully polished surfaces. The hardness (HV) was calculated from the diagonal length of the indentation determined by optical microscope observations using the equation according to ASTM C1327.

Toughness measurements, K_{IC}, were done by the four point bending test with a bar notched in the center. The equipment used in this study combined a bending test apparatus (Kammrath & Weiss bending module) with SEM providing sufficient magnification to be able to observe a propagating crack. The details on this study are summarized in our previous work [36]. The elastic properties of silicon nitride (the Young's modulus, E, and the Poisson's ratio, ν) are taken from [38].

According to FE results, plastically deformed zone, is the central area, underneath the indent print. According to modelling results this area is under compressive pressure and therefore it is crack free. So, this area is defined between the radial cracks – and has been measured using progressive polishing.

5. Results and discussions

In the current chapter the numerical results of both FE models, described in the Section 3, are included. Initially, the results of the fracture mechanics based model, investigating the DP plasticity effect, and later the results of the model based on the stress criterion are presented. The results of both models are compared to the experimental observations in terms of the Vickers cracks morphology.

The results of the indentation simulation are presented in Fig. 9, in terms of the average contact pressure, p_{avg}, as the function of the indentation load, P. The average contact pressure is evaluated by dividing the indentation load by the contact zone area, as follows from Eq. (6). Consistently with the dimensionless analysis (see Section 2), the average contact pressure is independent on the indentation load, as is shown in Fig. 9. Some points on the graph, corresponding to relatively low load, are slightly below the "saturated value", which is caused by numerical inaccuracy: if P is too low (somewhat below 1 [kgf]), then the amount of elements in contact is not sufficient to provide a good numerical solution. It is also indicated by Fig. 9 that the average contact pressure (or the material resistance to indentation) increases with the angle β, because according to the DP model the friction angle causes material strengthening under compressive stress which is predominant in an indentation contact (see Eq. (1) and Fig. 2).

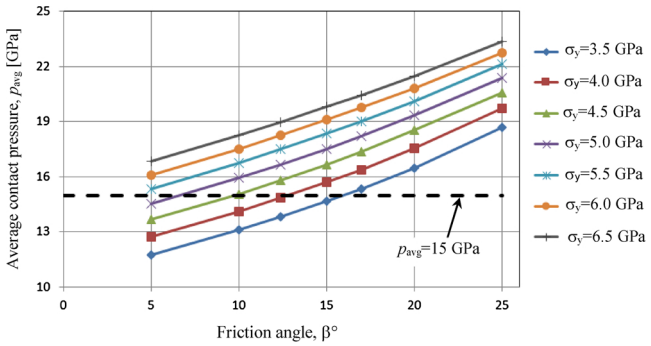

Fig. 10. The effect of the DP model parameters on the average contact pressure.

The effect of the DP model parameters (β and σ_y) on the average contact pressure is studied and presented in Fig. 10. Consistently with the DP model the average contact pressure, p_{avg}, gets higher as the friction angle, β, and the yield limit, σ_y, increase. The intersection of the curves in Fig. 10, with the straight dashed line $p_{avg} \equiv 15$ [GPa], defines the σ_y and β combinations, corresponding to the current ceramics (recall, that the hardness of Si_3N_4 used for hybrid bearings is around 15 [GPa], which is close to the hardness value reported in [19]). Namely, for these combinations of σ_y and β the radial crack formation due to the Vickers indentation is modelled based on the fracture mechanics analysis.

The distribution of K_I at the surface tip of the crack (termed here as K_I^0) is presented in Fig. 11 as the function of the surface crack length, C_R. The intersection of the K_I^0 vs. C_R curve with the straight line $K_I^0 \equiv K_{IC}$, predicts the size of the crack based on the fracture mechanics criterion described in the Section 3. The results presented in Fig. 11 correspond to the indentation of 10 [kgf], and as is indicated by this figure, the predicted crack length, C_R, decreases as the DP effect gets lower (in

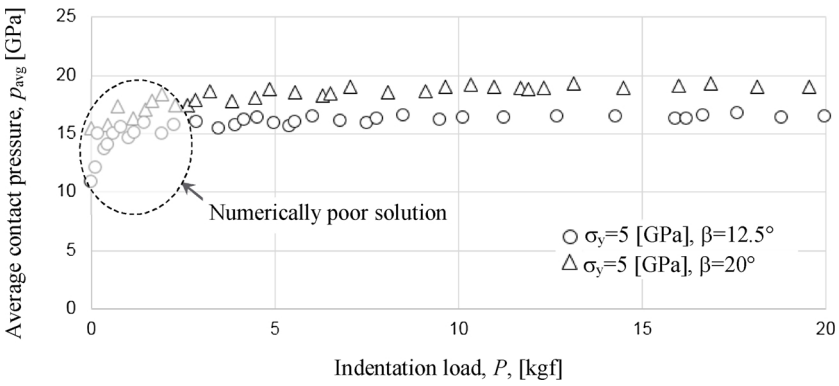

Fig. 9. Results of the FE simulation of indentation – the average contact pressure, p_{avg}, vs. the indentation load, P.

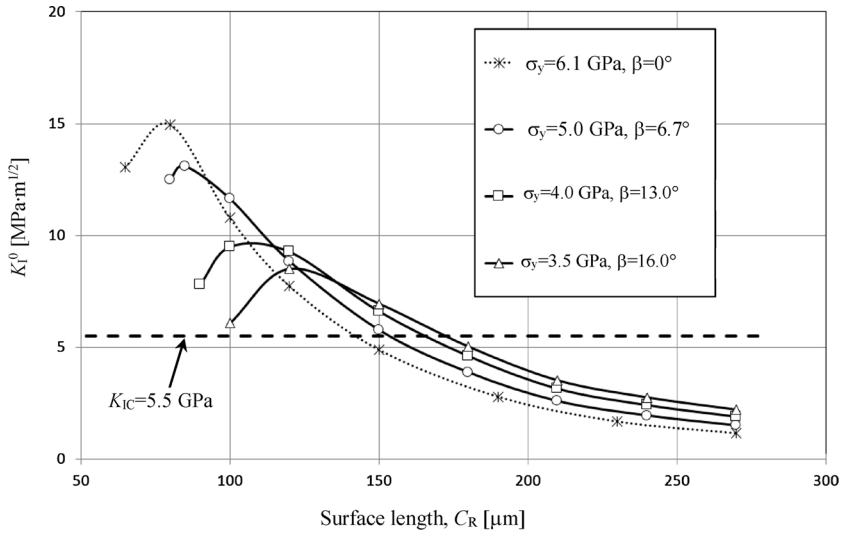

Fig. 11. The effect of the DP model parameters on the crack size.

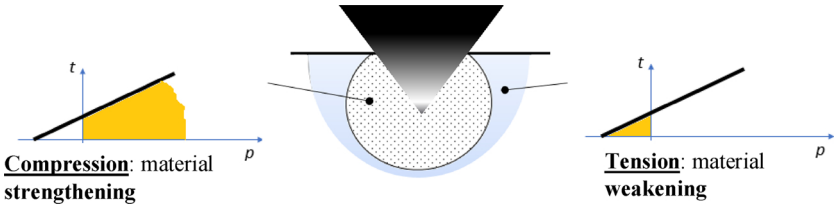

Fig. 12. Schematic of DP plasticity effect in the Vickers indentation.

the other words, the friction angle β decreases). Such effect can be explained in terms of the particular stress field, obtained in the Vickers indentation contact. The plastic zone is surrounded by tensile stresses, which according to the DP model causes weakening of material and its yielding (see Fig. 12). As result, larger material volume is involved in the plastic zone and therefore the tensile stress zone (surrounding the plastic zone) and the crack size, C_R, are also larger. In the case of the J_2-platcity, the plastic zone is smaller and the tensile stresses are concentrated in a smaller zone, which leads to higher K_I^0 value at the peak, as is shown in Fig. 11. Another effect contributing to this phenomenon is the volume expansion in the plastic regime (dilation), which is supposed to causes increase of the plastic and the tensile stress zone. The dilation is inherent to the associated DP plasticity ($\beta = \Psi$) and is absent in the case of J_2-plasticity, postulating volume conservation in the plastic regime.

By comparing the results in Fig. 11 to the micrograph in Fig. 13, presenting the residual indent and the cracks after 10 [kgf] Vickers indentation, it is apparent that the best numerical prediction is obtained for the material obeying the simple J_2-plasticity ($\beta = 0°$): the materials accounting for the DP behavior overestimate the surface length of the crack. The following physical interpretation can be attributed to this observation. The DP behavior is condition by the microstructure heterogeneity, which typically due to material imperfections causes the reduction of yield limit under tension. However, the Si_3N_4 ceramics used for the hybrid is sufficiently densified in order to prevent the existence of relatively large detrimental porosities. On the other hand, the volume of plasticized material is quite microscopic and therefore has low probability to contain these imperfections. Thus, the material response in the plastic range under either tension or compression is supposed to be similar.

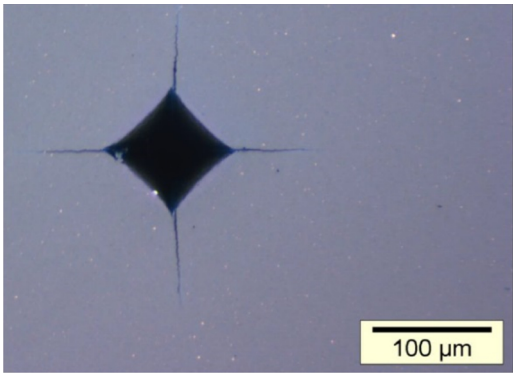

Fig. 13. Radial cracks formed in the Vickers indentation of 10 [kgf]. The surface size of the crack from tip to tip, $2C_R$, is around 280 [μm].

The Vickers indentation with the J_2-plasticity model is further explored by considering different values of σ_y, which influences the average contact pressure (or hardness). As follows from Eq. (7), K_I has to be normalized by $\sigma_y \cdot C_R^{1/2}$ or by $p_{avg} \cdot C_R^{1/2}$, because p_{avg} similarly to hardness, can be seen as the material property characterizing the plastic behavior of material; the surface crack length, C_R, according to Eq. (7), is normalized by the indent size, d. This normalization leads to the universal relation between the dimensionless K_I^0 and the dimensionless surface length of the crack, as is indicated by Fig. 14. Note, that according to Eq. (7) this relation can be dependent on the σ_y/E ratio, which is different for the three materials presented in Fig. 14, because σ_y changes from one material to another while E remains constant. However, in the given range of σ_y/E (which covers variations in E and σ_y in different Si_3N_4 grades) the influence of this ratio is subtle (as can be concluded from Fig. 14) and therefore can be neglected. Additional explanation for this effect is given in Fig. 15, presenting the distribution of the dimensionless residual stress σ_{yy} along the indented substrate surface (at $z = 0$). This tensile stress results in the radial crack formation by activating the opening mode K_I. As is indicated by the numerical results in Fig. 15, the dimensionless stress σ_{yy}/σ_y variation is negligible when the E/σ_y parameter varies in relatively narrow range (from $E/\sigma_y = 60$ to 80). Only when it is dramatically decreased (to $E/\sigma_y = 25$) the σ_{yy}/σ_y distribution is visibly modified, because by the increasing of

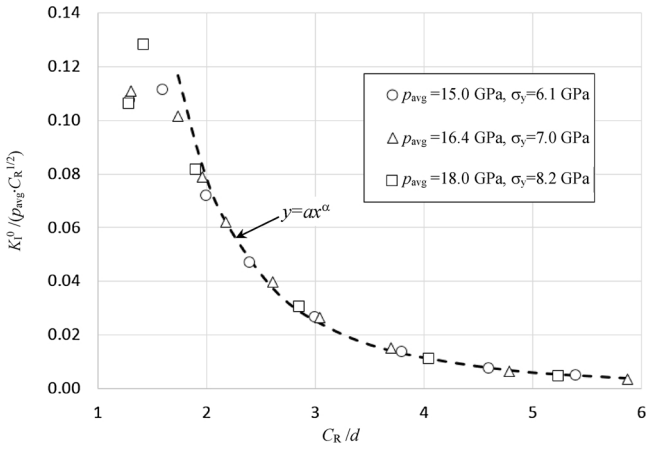

Fig. 14. Dimensionless K_I^0 vs. the dimensionless crack size for the indentation problem (P = 10 [kgf]) modeling by the J_2-plasticity. Due to the universal (independent on the material properties) relation between these dimensionless parameters the master curve (the dashed line, $y=ax^{\alpha}$) is defined.

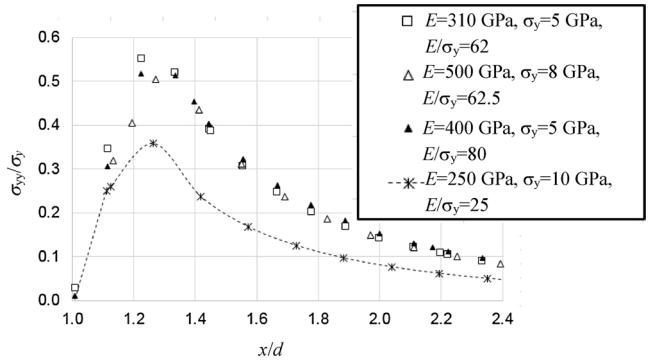

Fig. 15. Dimensionless distribution of the residual stress (P = 10 [kgf]), σ_{yy} (see Fig. 1b) activating the crack opening mode K_I.

σ_y and decreasing of E the indentation contact gets more elastic. In the other words, the amount of irreversible plastic deformations gets lower which results in the decreased level of tensile residuals stress. However again, concerning Si_3N_4 ceramics such low E/σ_y values are not typical, so the results in Fig. 14 can be universally used for the different grades of Si_3N_4, for which E and σ_y can indeed vary in a certain narrow range.

The master curve is defined by the best fitting of the numerical results in Fig. 14 to the empirical equation: $y=ax^{\alpha}$. Using this equation along with Eq. (6), a semi-analytical solution predicting the surface crack length, C_R, as the function of the indentation load, P, hardness, H, and toughness, K_{IC}, (of the indented Si_3N_4 substrate), can be developed. This solution is given in terms of the following empirical equation:

$$C_R = 0.48\frac{(P\bullet g)^{3/5}}{H^{1/5}K_{IC}^{2/5}} \times 1000 \tag{9}$$

In Eq. (9), $g \approx 9.8$ [m/sec^2] is used to convert the indentation load from the kilogram force to the units of Newton, and the term $\times 1000$ to convert the crack size from millimeters to microns. For consistency, the units [MPa] and [MPa·$mm^{1/2}$] are used for the hardness, H, and the toughness, K_{IC}, respectively, in Eq. (9). Finally note, that the powers in Eq. (9) are defined in such way that the units of length (corresponding to C_R) are satisfied in this equation (the coefficient 0.48 is unitless).

In Fig. 16 the comparison between the predicted crack length (solid line) and the experimental observations (markers) is presented. Recall, that the following properties were used for the prediction: K_{IC} = 5.5 [MPa·$m^{1/2}$] [36] and p_{avg} = 15 [GPa] which is close to the hardness of Si_3N_4 (see e.g. [19]). In the current work eight Si_3N_4 samples were tested: three samples for the load of 10 [kgf], two samples for 5 [kg]

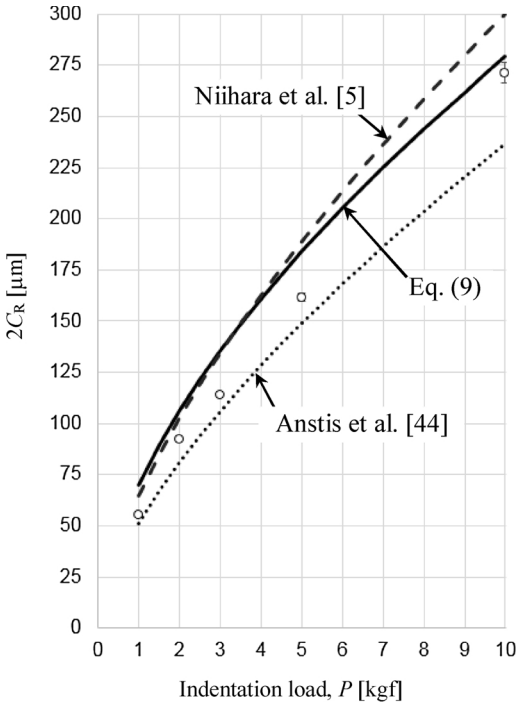

Fig. 16. Surface length of the crack vs. indentation load. The lines correspond to modelling results and the markers to the experimental data.

and one sample for 3, 2 and 1 [kgf]. As is shown in Fig. 16, the model slightly overestimates the surface length of the crack, especially at low load, which can be resulted by the main model assumption stating that the radial crack is formed by residual stress at the instance of unloading completion. In reality, however, the crack can initiate during the loading stage and by this cause stress relaxation which is supposed to reduces amount of plasticity and the level of residual stresses. In the other words, according to the current model the residual stress is exaggerated which eventually leads to the crack size overestimation. It can also be related to the fact that under low load, some considerable deviation of the average contact pressure from the hardness can take place. Recall, that the theoretical basis behind the simulation requires that the stress distribution is independent on the load, which can be not the case under low load as effect of different material response at small scale. Moreover, at low load crack can have geometrical configuration which is different from the currently assumed radial crack [22].

The modeling results are presented in Fig. 17 along with the experimental data for relatively high level of indentation loads: 15, 20 and 30 [kgf]. The experimental results in Fig. 17 are reported in [8]; among other things, this work explores Vickers indentation of Si_3N_4

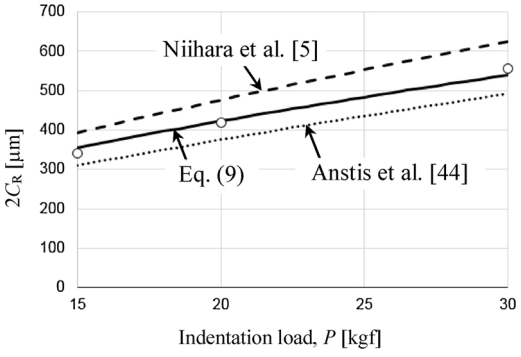

Fig. 17. Surface length of the crack vs. indentation load. The experimental results are taken from [8]. The lines correspond to modelling results and the markers to the experimental data.

Table 1
Equations used in literature for the evaluation of indentation fracture toughness.

Reference	Equation
Anstis et al. [44]	$K_{IC} = 0.016\frac{P}{C_R^{3/2}}\left(\frac{E}{H}\right)^{1/2}$
Niihara et al. [5]	$K_{IC} = 0.0309\frac{P}{C_R^{3/2}}\left(\frac{E}{H}\right)^{2/5}$

used for hybrid bearings. It is interesting to note, that the crack size overestimation provided by the current model, decreases as the contact load increase. For example, according to Fig. 17, the difference between the experiment and the prediction is around 20% for the load of 1 [kgf], while for the load of 10 [kgf] it is less than 5%. Furthermore, in Fig. 17 (presenting C_R for high indentation load) the modeling and the experimental results are very close to each other. Such phenomenon can be probably explained by keeping in mind that Si_3N_4 is a heterogeneous material and in addition to plastic deformation can accumulate damage (see e.g. [40]). As the indentation load increases, the size of stressed volume and the amount of microscopic imperfections and damages in this volume increase, too. This can lead to the reduction of hardness (see [41,42]), and as result to larger indent and larger length of the radial crack, C_R.

Finally, the crack size prediction by Eq. (9) is tested against other two equations presented in literature (see Table 1). These equations (among many others [43]) are used for the evaluation of indentation fracture toughness based on the radial crack size. By rearranging these equations, C_R vs. the indentation load, P, can be evaluated. As is indicated by Figs. 16 and 17, the prediction by the current equation is closer to the experimental results (especially at high load), compared to the previously developed equations. For the given material, the equation proposed by Anstis et al. [44] underestimate the experimental results, while the equation by Niihara et al. [5] overestimates them.

The results of the stress criterion based model, simulating the propagation of radial crack during the loading-unloading process are presented in Fig. 18. In the current work, this model utilizes only J_2-plasticty, because as was found by the previous model, J_2-plasticty provides more adequate results (compared to the experiment), than the DP plasticity. The load-displacement curve, corresponding to this simulation is shown in Fig. 19. The markers in Fig. 19 are denoted by the Latin letters (varying from (a) to (e) during the loading and from (e) to (h) during the unloading stage), and each letter corresponds to one of the "snapshots" demonstrated in Fig. 18. The curve in Fig. 19 presents

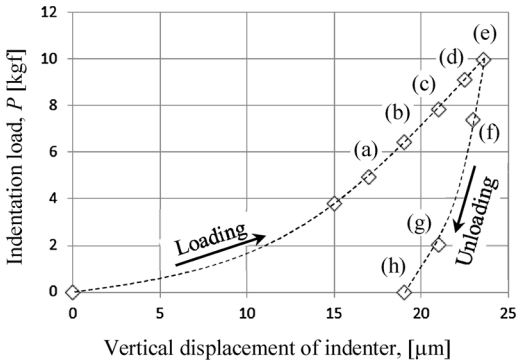

Fig. 19. Indentation load vs. vertical displacement of indenter during the loading-unloading process. Each marker presented in the figure corresponds to a certain instance in Fig.18.

the indentation load, P, as the function of the vertical displacement of the indenter (in z-direction, see Fig. 6); the area below the loading part of the curve defines the work invested in the indentation and the area below the unloading part defines the work gained back during the unloading stage. The load, P, as is shown in Fig. 19, increases up to the maximum load of 10 [kgf], from which the unloading stage begins. The bright contrast on Fig. 18 corresponds to the crack domain, and the dark one to the un-cracked zone. The red color zones in Fig. 18 indicate the "healed" portion of the crack at which its faces are in the contact with each other due the compressive stresses in a plastic zone. This portion is developed during the loading stage by the gradual engagement of the crack into the expanding plastic zone.

A radial crack, as is shown in Fig. 18a, initiates during the loading stage, somewhere at P equal to 5 [kgf] (see Fig. 19). The radial crack extends during the loading stage (see Fig. 18b–e), as the load P increases. The crack extension continues during the unloading stage, too (see Fig. 18f–h), because during this stage tensile stress intensifies, which leads to the further material cleavage and crack propagation. The complex morphology of the Vickers cracking (including an indent, radial cracks and a plastic zone) predicted by the stress criterion based model, is compared to the experimentally measured morphology. This morphology was reconstructed by gentle polishing of the Vickers indented sample and taking images after each material removal step (see Fig. 20). Few indented samples were investigated and the Max-Min range and the averaged value of each geometrical parameter was estimated (see the table of Fig. 21). The FE results presented in Fig. 18h (at the completion of the unloading stage) are compared to the

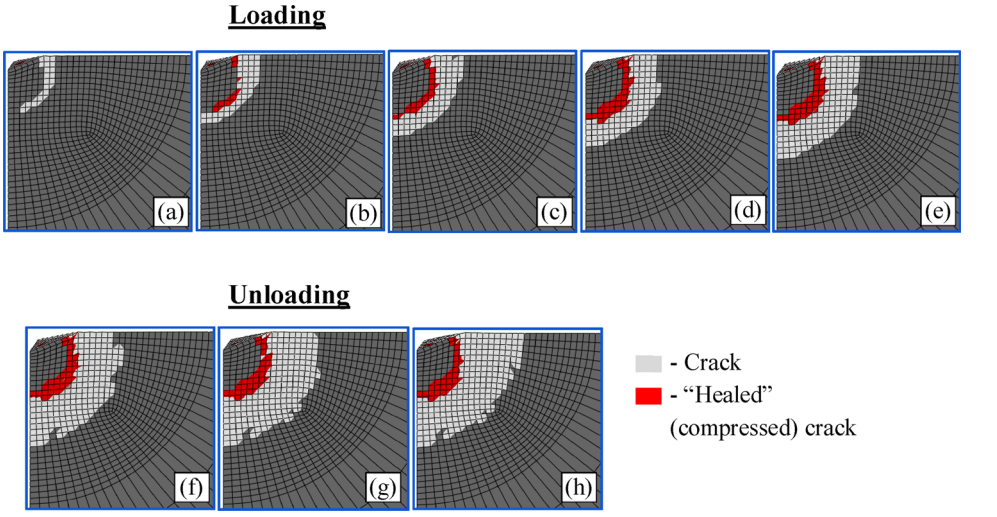

Fig. 18. Crack propagation during the loading-unloading process.

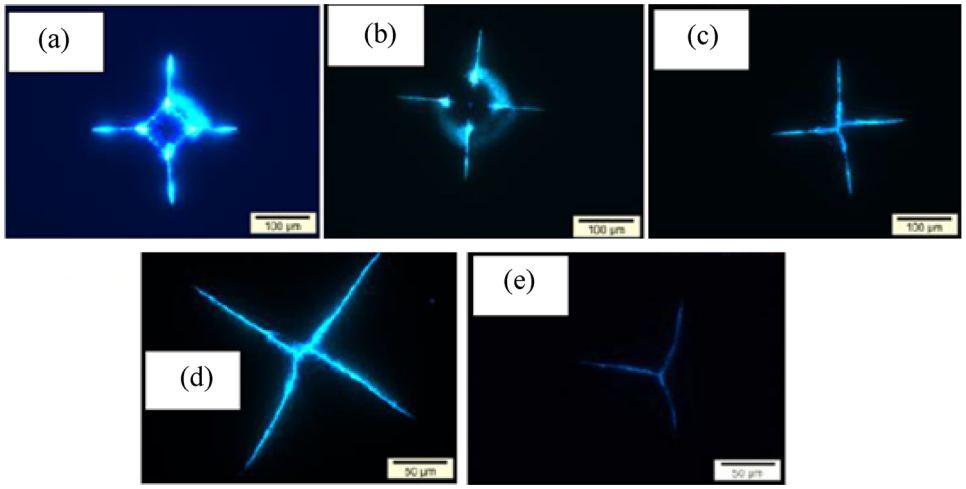

Fig. 20. Fluorescent penetrating images of the 10 [kgf] Vickers indented Si_3N_4 sample. The images are taken during the progressive polishing for the removed material thickness of 10 [μm] (b), 40 [μm] (c), 50 [μm] (d), 80 [μm] (e) and an unpolished sample (a).

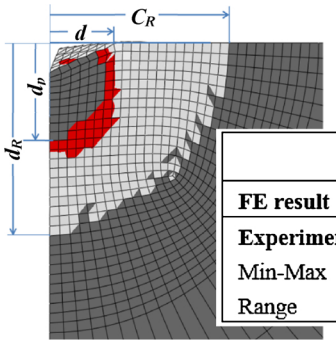

	d [μm]	C_R [μm]	d_R [μm]	d_p [μm]
FE result	**53**	**133**	**130**	**60**
Experiment	**≈ 50**	**130**	**120**	**25**
Min-Max Range	-----	126-135	108-133	15-35

Fig. 21. The morphology of radial crack – modeling results vs. experiment.

experimental measurements in terms of the following geometrical parameters (see Fig. 21): the surface crack length, C_R, the crack depth, d_R, the indent size, d, and the plastic zone depth, d_p. The comparison indicates good agreement between the theoretical predictions and the experimental data in terms of the indent size, d, crack length, C_R, and depth, d_R. However, the plastic zone depth, d_p, is overestimated by FE, which can be explained due to a numerical imperfection in the model: at very low indentation loads the amount of elements in the stressed zone is too small to model properly the formation of cracks at this stage. This means that in reality, the radial crack forms earlier and therefore the plastic zone is shallower than predicted. Another possible reason is the inaccuracy in the experimental measurement of the plastic zone geometry.

6. Conclusions

The theoretical study of Si_3N_4 cracking under the Vickers indentation was conducted. This study proposes two methods for the simulation of radial crack formation: the first method is based on fracture mechanics and the second one on the tensile stress criterion. The crack formation in Vickers indentation is driven by plastic deformation which limited amount can occur even in such non-ductile materials as Si_3N_4 ceramics. Due to limited knowledge on the Si_3N_4 plasticity, the DP model was used, because this model being more general than the classical J_2-plasticity is frequently utilized for non-metallic materials. The results of the fracture mechanics based model in terms of the surface crack length were compared to the experimentally measured length, which can be easily identified. It was found that the DP behavior of material in plastic range results in overestimation of the crack size and that the best prediction is achieved when the DP effect diminishes and the plastic behavior of Si_3N_4 converges to the classical J_2-plasticity. Probably, it is due to small-scale plasticity in indentation and good quality of the Si_3N_4 ceramics used for the hybrid bearings, which by having high densification level and fine structure, prevents the existence of heterogeneity causing the DP behavior (relatively large porosities and other defects). The results of the stress criterion based model (run for J_2-plasticity) were compared to the results of a destructive test by which the complex morphology of the Vickers indented zone can be visualized. The good correlation between the modeling and experimental results was found in terms of the crack geometry and the indent size.

References

[1] L. Wang, R.W. Snidle, L. Gu, Rolling contact silicon nitride bearing technology: a review of recent research, Wear 246 (1-2) (2000) 159–173.
[2] R.H. Vegter, J.T. Slycke, The role of hydrogen on rolling contact fatigue response of rolling element bearings, J. ASTM Int. 7 (2) (2009) 1–12.
[3] Y. Kadin, Modeling of hydrogen transport in static and rolling contact, Trib. Trans. 58 (2) (2015) 260–273.
[4] C. Vieillard, Y. Kadin, G.E. Morales-Espejel, A. Gabelli, An experimental and theoretical study of surface rolling contact fatigue damage progression in hybrid bearings with artificial dents, Wear 364–365 (2016) 211–223.
[5] K. Niihara, R. Morena, D.P.H. Hasselman, Evaluation of KIC of brittle solids by the indentation method with low crack-to-indentation ratios, J. Mater. Sci. Lett. 1 (1) (1982) 13–16.
[6] K. Kida, T. Urakami, T. Yamazaki, K. Kitamura, Surface crack growth of silicon nitride bearings under rolling contact fatigue, Fatigue Fract. Eng. Mater. Struct. 27 (2004) 657–668.
[7] K. Kida, T. Honda, E.C. Santos, Mode II surface crack growth under rolling contact fatigue and cyclic shear stress in Si3N4, WIT Trans. Eng. Sci. 76 (2012) 175–187.
[8] R.J.F. Hanzal, Rolling Contact Fatigue Failures in Silicon Nitride and Their Detection. Thesis for the Degree of Doctor of Philosophy, University of Southampton, 2013.
[9] Z. Chen, X. Wang, A. Atkinson, N. Brandon, Spherical indentation of porous

ceramics: cracking and toughness, J. Eur. Ceram. Soc. 36 (2016) 3473–3480.
[10] Y. Tang, A. Yonezu, N. Ogasawara, N. Chiba, X. Chen, On radial crack and half-penny crack induced by Vickers indentation, Proc. R. Soc. A 464 (2008) 2967–2984.
[11] X. Chen, J.W. Hutchinson, A.G. Evans, The mechanics of indentation induced lateral cracking, J. Am. Ceram. Soc. 88 (5) (2005) 1233–1238.
[12] H.G. Hyun, F. Rickhey, J.H. Lee, J.H. Hahn, H. Lee, Characteristics of indentation cracking using cohesive zone finite element techniques for pyramidal indenters, Int. J. Solids Struct. 51 (2014) 4327–4335.
[13] A. Yonezu, T. Hara, T. Kondo, H. Hirakata, K. Minoshima, Evaluation of threshold stress intensity factor of hydrogen embrittlement cracking by indentation testing, Mater. Sci. Eng. A 531 (2012) 147–154.
[14] F. Rickhey, K.P. Marimuthu, H. Lee, Investigation on indentation cracking-based approaches for residual stress evaluation, Materials 10 (4) (2017) 1–16.
[15] J.H. Lee, Y.F. Gao, K.E. Johanns, G.M. Pharr, Cohesive interface simulations of indentation cracking as a fracture toughness measurement method for brittle materials, Acta Mater. 60 (2012) 5448–5467.
[16] S.R. Rani, N.K. Prasad, S.T. Krishna, Applicability of Mohr-Coulomb & Drucker-Prager models for assessment of undrained shear behavior of clayey soils, Int. J. Civil Eng. Technol. 5 (10) (2014) 104–123.
[17] T. Yu, J.G. Teng, Y.L. Wong, S.L. Dong, Finite element modeling of confined concrete-I: Drucker–Prager type plasticity model, Eng. Struct. 32 (3) (2010) 665–679.
[18] K. Liu, S.L. Chen, Finite element implementation of strain-hardening Drucker–Prager plasticity model with application to tunnel excavation, Undergr. Space 2 (2017) 168–174.
[19] S.K. Ajjarapu, J.A. Patten, H. Cherukuri, C. Brand, Numerical simulations of ductile regime machining of silicon nitride using the Drucker-Prager material model, Proc. Inst. Mech. Eng. 218 (2004) 577–582 Part C: J. Mech. Eng. Sci..
[20] J.J. Kruzic, D.K. Kim, K.J. Koester, R.O. Ritchie, Indentation techniques for evaluating the fracture toughness of biomaterials and hard tissues, J. Mech. Behav. Biomed. Mater. 2 (2009) 384–395.
[21] F.R. Cook, M.G. Pharr, Direct observation and analysis of indentation cracking in glasses and ceramics, J. Am. Ceram. Soc. 73 (4) (1990) 787–817.
[22] T. Lube, Indentation crack profiles in silicon nitride, J. Eur. Ceram. Soc. 21 (2001) 211–218.
[23] D.M. Marsh, Plastic flow in glass, Proc. R. Soc. Lond. Ser. A Math. Phys. Sci. 279 (1378) (1964) 420–435.
[24] K.L. Johnson, The correlation of indentation experiments, J. Mech. Phys. Solids 18 (1970) 115–126.
[25] Y. Kadin, A.V. Rychahivskyy, Modeling of surface cracks in rolling contact, Mater. Sci. Eng. A 541 (2012) 143–151.
[26] K.E. Johanns, J.H. Lee, Y.F. Gao, G.M. Pharr, An evaluation of the advantages and limitations in simulating indentation cracking with cohesive zone finite elements, Modell. Simulat. Mater. Sci. Eng. 22 (1) (2013).
[27] L. Kogut, I. Etsion, Elastic-plastic contact analysis of a sphere and a rigid flat, J. Appl. Mech. 69 (2002) 657–662.
[28] B. Zohuri, Dimensional Analysis Beyond the Pi Theorem, 1st ed., Springer, 2017.
[29] D. Tabor, The Hardness of Metals, Oxford University Press, New York, NY, 1951.
[30] P. Clément, S. Meille, J. Chevalier, C. Olagnon, Mechanical characterization of highly porous inorganic solids materials by instrumented micro-indentation, Acta Mater. 61 (2013) 6649–6660.
[31] M. Rodríguez, J.M. Molina-Aldareguía, C. González, J.L. Lorca, Determination of the mechanical properties of amorphous materials through instrumented nanoindentation, Acta Mater. 60 (9) (2012) 3953–3964.
[32] M.N.M. Patnaik, R. Narasimhan, U. Ramamurty, Spherical indentation response of metallic glasses, Acta Mater. 52 (2004) 3335–3345.
[33] S. Suresh, Fatigue of Materials, Cambridge University Press, 1998.
[34] D. Taylor, The Theory of Critical Distances: A New Perspective in Fracture Mechanics, Elsevier, 2007.
[35] S. Fünfschilling, T. Fett, M.J. Hoffmann, R. Oberacker, T. Schwind, J. Wippler, T. Böhlke, H. Özcoban, G.A. Schneider, P.F. Becher, J.J. Kruzic, Mechanisms of toughening in silicon nitrides: the roles of crack bridging and microstructure, Acta Mater. 59 (2011) 3978–3989.
[36] Y. Kadin, S. Strobl, C. Vieillard, P. Wijnbergen, V. Ocelik, In-situ observation of crack propagation in silicon nitride ceramics, Procedia Struct. Integr. 7 (2017) 307–314.
[37] Y. Kadin, M. Mazaheri, C. Vieillard, S. Strobl, P. Wijnbergen, V. Ocelik, Modelling of Crack Formation Under Vickers Indentation in Silicon Nitride Ceramics. New Trends in Fatigue and Fracture, Lisbon, Portugal (2018).
[38] S. Strobl, T. Lube, P. Supancic, O. Schöppl, R. Danzer, Surface strength of balls made of five structural ceramic materials evaluated with the Notched Ball Test (NBT), J. Eur. Ceram. Soc. 37 (2017) 5065–5070.
[39] Y.F. Gao, A.F. Bower, A simple technique for avoiding convergence problems in finite element simulations of crack nucleation and growth on cohesive interfaces, Modell. Simul. Mater. Sci. Eng. 12 (2004) 453–463.
[40] S.M. Taheri Mousavi, N. Richart, C. Wolff, J.F. Molinari, Dynamic crack propagation in a heterogeneous ceramic microstructure, insights from a cohesive model, Acta Mater. 88 (2015) 136–146.
[41] A. Mkaddem, R. Bahloul, P. Dal Santo, A. Potiron, Experimental characterization in sheet forming processes by using Vickers micro-hardness technique, J. Mater. Process. Technol. 180 (2006) 1–8.
[42] C.C. Tasan, J.P.M. Hoefnagels, M.G.D. Geers, Identification of the continuum damage parameter: an experimental challenge in modeling damage evolution, Acta Mater. 60 (2012) 3581–3589.
[43] D. Ćorić, L. Ćurković, M.M. Renjo, Statistical analysis of Vickers indentation fracture toughness of Y-TZP ceramics, Trans. Famena (2017) XLI-2.
[44] G.R. Anstis, P. Chantikul, B.R. Lawn, D.B. Marshall, A critical evaluation of indentation techniques for measuring fracture toughness: I, direct drack measurements, J. Am. Ceram. Soc. 64 (9) (1981) 533–538.